Report
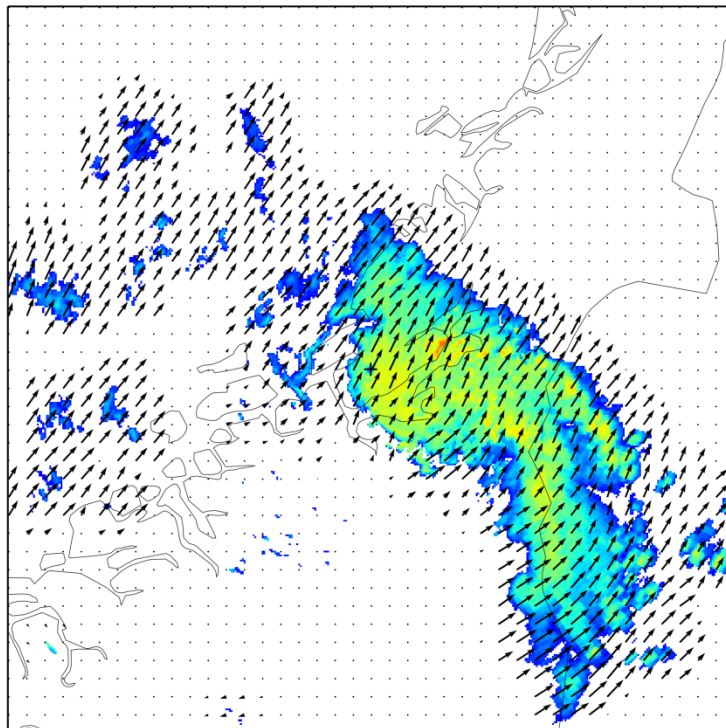
A preliminary investigation of the potential of radar-based short-term precipitation forecasting in central Norway

An experiment on using Lagrangian persistence for nowcasting of two events

Author
Yisak Sultan Abdella
Lena S. Tøfte

SINTEF Energy Research
Energy Systems
2013-11-28

SINTEF

KEYWORDS:

Report

A preliminary investigation of the potential of radar-based short-term precipitation forecasting in central Norway

An experiment on using Lagrangian persistence for nowcasting of two events

VERSION	DATE
1	2013-11-28

AUTHOR(S)
Yisak Sultan Abdella
Lena S. Tøfte

CLIENT(S)	CLIENT'S REF.
Trondheim Kommune	Olav Nilssen
Regionalt Forskningsfond Midt-Norge	Kari Merete Andersen

PROJECT NO.	NUMBER OF PAGES:
12X846	34

ABSTRACT

An experiment on using Lagrangian persistence for nowcasting of two events

Flood predictions in urbanized catchments require forecasting systems with higher spatial resolution and faster updating frequency. Radar-based short-term forecasting techniques have the potential of fulfilling these requirements. In this study, a nowcasting technique based on advection of radar images has been tested on two events over central Norway. The test shows that Lagrangian persistence performs significantly better than the simple Eulerian persistence for both events indicating that advection is a very important factor for successfully predicting the events. The performance measures calculated for the minimum reflectivity threshold of 7dBZ generally indicate good predictability of the storm envelops when compared with the same measures obtained in other studies. For each event, it is found that the nowcast skill decreases with the forecast lead time, increases with the verification area used around a forecast location, and decreases with higher radar reflectivity thresholds.

PREPARED BY	SIGNATURE
Yisak Sultan Abdella	*Yisak Abdella*
CHECKED BY	SIGNATURE
Sjur A. Kolberg	*Sjur Kolberg*
APPROVED BY	SIGNATURE
Magnus Korpås	*Magnus Korpås*

REPORT NO.	ISBN	CLASSIFICATION	CLASSIFICATION THIS PAGE
TR A7379	978-82-594-3580-4	Unrestricted	Unrestricted

Document history

VERSION	DATE	VERSION DESCRIPTION
1	2013-11-28	Final version

Samandrag

Bakgrunn

Trondheim og andre bykommunar treng betre driftsplanleggingsverktøy for flaum- og overvatn. Klimaendringar og byfortetting gjer at eksisterande avløpsnett har fått aukande kapasitetsproblem. Eit viktig tiltak er å kunne varsle kraftige regnbyger i tide til at basseng og fordrøyingsvolum som vatnet blir leia gjennom for å unngå flaum, kan tappast ned i forkant. Tradisjonelle varslingsmodellar (dvs atmosfæremodellar) egnar seg dårleg for denne typen korttidsvarsling som krev høg romleg oppløysing og raskare oppdateringsfrekvens. Derimot gjev verradar av typen installert i Norge momentanbilete av nedbøren kvart 15. minutt, så korttidsprognoser frå verradar vil kunne vere avgjerande input til kommunale planleggingsverktøy. Det er frå andre studiar kjend at radarbaserte framskrivingar/ekstrapolering gjev betre prognoser enn numeriske atmosfæremodellar for leietider under tre timar. I dette prosjektet har vi testa om data frå nedbørradar kan brukast til slik korttidsvarsling av intense og kraftige regnbyger, såkalla nowcasting.

Analysane

To nedbørepisodar som førde til alvorleg flaum i Trondheim er brukt i studien, 13 august 2007 og 28 juni 2010. Det er utvikla ein statistisk prognosemodell basert på radardata frå Rissa-radaren, der metodar frå rom-tid-statistikk er brukt og evaluert i høve til kor gode prognosane blir for nedbørepisodar av ulik varighet, og for ulike leietider ved varsling av episodane

Begge dei studerte episodane hadde konvektive eigenskapar med høg nedbørintensitet. I studien vart følgjande gjort:

1. Adveksjonsvektoren mellom etterfølgjande refleksjonsbilete vart berekna: global vektor vha ein maksimums krysskorrelasjonsteknikk, og fordelt adveksjonsvektor med ein optisk flytalgoritme.
2. Varsel med leietider på opp til 2 timar med 15 minutts intervall vart generert ved bruk av global adveksjonsvektor. Prediksjonsdomenet var ein 200×200 km^2 region rundt Rissa-radaren med romleg oppløysing av varsla på 1×1 km^2.
3. Seks prestasjonsmål vart berekna ved å samanlikne varsla og observerte radarbilete. Dette vart gjort for fleire terskelverdiar for refleksjon (7, 25, 30, 35 og 40 dBZ, grovt tilsvarande 0.1, 1, 3, 6 og 12 mm/time) og verifiseringsområder (1×1, 3×3, 5×5, 7×7, 9×9 og 11×11 km^2) for å analysere skalaavhengigheten til prediksjonane.
4. For nokre få tidssteg vart global adveksjonsvektor samanlikna med fordelte vektorfelt estimert for same tidssteg for å vurdere representativiteten til romleg uniform adveksjon.

Resultat og konklusjonar

Generelt viser studien at ein kan oppnå gode varsel for utbreiing av kraftige nedbørepisodar ved bruk av radardata i nowcasting. Resultata viste at adveksjon (romleg bevegelse) er ein svært viktig faktor for å kunne prognosere hendingane korrekt. Dette stiller krav til kva slags modell som blir brukt.

Euler-modellen for persistens (stabilitet) seier at forholda er stabile, anten som nivå eller som trend. Vêret om ein time blir altså varsla som anten det same som no, eller som at noverande utvikling fortsett. Det er ingen romleg bevegelse med i modellen, dvs at ei regnbye som flytter seg mellom to tidspunkt blir modellert som minkande nedbør ein stad og veksande nedbør ein annan. Langrange-modellen legg og vekt på persistens, men her er i tillegg romleg bevegelse med i modellen. Det vil seie at vêret om ein time kan

varslast som no, men flytta 12 km mot nordaust. Mange vêrsituasjonar kan skildrast enklare og betre med Lagrange-modellen enn med Euler-modellen.

Resultata viser at metodar som inkluderer adveksjon (Lagrange-modellen) gjev signifikant betre simuleringar enn metodar som ikkje inkluderer romleg bevegelse (Euler-modellen). Samtidig kan bruk av global adveksjonsvektor føre til feilaktige varsel for lengre leietider når nedbørepisoden har konvektive trekk med signifikant ulike bevegelsar internt, og bruk av fordelte vektorar i adveksjonsberekningane kan av og til gje urealistisk stor dispersjon i det varsla feltet.

Dei to analyserte nedbørepisodane hadde ulik utviklingshastigheit og utbreiing i rommet, begge deler speler ei viktig rolle for kor godt ein kan varsle hendinga. For begge episodane og uavhengig av metode vil storleiken på verifiseringsområdet bety noko: når dette aukar frå eit enkeltpiksel (1 km^2) til opp mot ein region på 11 x 11 pikslar (121 km^2) blir resultata gradvis betre. Derfor er det eit poeng at storleiken på verifiseringsområdet blir sett basert på kva slags krav ein har til geografisk treff for varsla.

Kva slags terskelverdi ein bruker for minimumsrefleksiviteten er også viktig. Terskelverdiar på 7, 25, 30, 35 og 40 dBZ (grovt tilsvarande 0.1, 1, 3, 6 og 12 mm/time) vart brukt, og generelt viser det seg at ein grenseverdi på 7 dBZ vil gje god prediktabilitet for utbreiinga av nedbørhendingane. Med høgare grenseverdi for minimumsrefleksiviteten minkar varslingstreffsikkerheiten for begge episodane. Dette viser at meir intense trekk ved nedbørfeltet har liten romleg utbreiing og derfor er vanskelege å predikere. Dette gjev konsekvensar for bruk av nowcasting/korttidsvarsling i urbane flaumvarslingssystem sidan det er dei mest intense hendingane som er viktigast i den samanhengen.

Resultata vart vist fram og diskutert på ein todagars workshop med nowcasting- og nedbørekspertar frå Norge, England og Italia, og norske brukarar frå kommunar, vegvesen og Jernbaneverk. Workshopen viste at problemstillinga er høgrelevant også i Norge, og at problema rundt urban flaum, jordskred i små nedbørfelt som konsekvens av intensiv nedbør, og store snøfall i urbane område, er aukande. For nedbør i form av regn har metodikken som kan brukast i varslingssystem kome lenger enn for snø, som er meir komplisert i radarsamanheng.

<u>Vidare arbeid</u>

I vidare arbeid er det fleire moment som bør undersøkast:
- Med lengre leietider er det data langt unna radaren som blir brukt, desse er også mest påverka av kjende feilkjelder.
- Både for datakvaliteten generelt og med lenger leietider spesielt vil det kunne vere fordelar å ved å bruke ein mosaikk av fleire radarar i staden for ein enkeltradar som i denne studien.
- Dei største urbane flaumane er vanlegvis generert av konvektive nedbørepisodar karakterisert ved høg intensitet og liten romleg utbreiing, dette er også dei episodane som er vanskelegast å varsle. Det vil derfor vere viktig å evaluere varslingsmetodar mot episodar av denne typen.
- Det vil vere nyttig å vite meir om kor lenge ein typisk småskala konvektiv episode varar, både for å setje grenser for ekstrapolering i tid og for å kunne modellere.
- Ved å inkludere fleire kjelder enn radardata vil ein kunne berekne den fordelte adveksjonsvektoren også i ruter utan nedbør og redusere usikkerheita.
- Ved bruk av både global og fordelt adveksjonsvektor blir varsel berekna med utgangspunkt i at vektorfeltet er stasjonært i tid, det bør undersøkast i kva slags situasjonar og i kor stor grad dette er riktig.

Table of contents

1 Introduction

Quantitative precipitation forecasting (QPF) is an important area of research within hydrology where the major aim is to improve the accuracy and increase the useful lead time of flood and flash-flood warning systems. For the flood prediction of large catchments with areal extents in the order of several thousands of square kilometres and response times in the order of several hours to days, the large scale QPFs by Numerical Weather Prediction models are usually sufficient to at least assess general trends. However, their probability to fail gets higher when moving to prediction in small urban catchments. The smaller sizes of urban catchments combined with the fast and strong sensitivity of their responses to the variations of precipitation pose a challenge. A reasonable QPF in such catchments requires a precise estimation of the initial states which is normally only achieved by direct observation and high spatio-temporal forecast resolution. Even when this requirement is fulfilled, an acceptable QPF quality is achieved only for forecast lead times of a few hours (0-3 hours).Short-term forecasting procedures with such short lead times are termed as "nowcasting".

In current operational nowcasting systems, extrapolation of radar echoes is one of the primary mechanisms that are used to generate forecasts in the 0-3 hours time frame. As summarized in Ruzanski et al. (2011), strictly radar-based nowcasting methods belong to one of the following four categories (or a combination thereof): area-based, object-based, statistical, and probabilistic approaches. Area-based nowcasting approaches estimate a motion vector field over the entire radar coverage domain and have shown effectiveness in estimating the translation of a variety of precipitation pattern types (Germann and Zawadzki 2002). Object-based nowcasting schemes attempt to identify areas of high reflectivity in radar fields and track the size, shape, and translation of coherent features in time across successive fields (Han et al. 2009). In order to incorporate knowledge of atmospheric dynamics, the statistical nowcasting methods represent atmospheric evolution by statistical models (Fox and Wikle 2005). Driven by the need for better description of uncertainty, the probabilistic approaches estimate the probability of encountering a precipitation rate above a certain threshold at each point in prediction domain (Dance et al. 2010).

A radar –based nowcasting technique which can be grouped under area-based methods has been investigated in this study. The main objective of the investigation is two fold: (1) to do a preliminary assessment of the potential of using such a method for short-term forecasting of precipitation over Trondheim, and (2) to identify key issues which should be investigated further in order to fully exploit this potential. The technique is based on Lagrangian persistence and has been tested on two precipitation events which occurred on 13 August 2007 and 28 June 2010.

The report is organized as follows. The forecasting technique is briefly described in section 2. Section 3 gives an overview of the data used, the prediction domain and the selected events. The various performance measures applied for evaluation of the forecasts are described in section 4. Results from the application of the technique on the two events are presented in section 5. In section 6, a summary is given and some conclusions are drawn based on the application on the events. Finally some issues for further research are identified and listed under section 6.

2 Forecasting technique

2.1 Formulation

Most of the radar-based QPF procedures may be described using the following two-dimensional conservation equation

$$\frac{dZ}{dt} = \frac{\partial Z}{\partial t} + \frac{\partial uZ}{\partial x} + \frac{\partial vZ}{\partial y} \qquad (1)$$

where $Z(x, y)$ is the radar reflectivity at the point (x, y), and u, v are the velocity components of the reflectivity field. When the compressibility term $Z(\partial u/\partial x + \partial v/\partial y)$ is neglected, Eq. (1) reduces to

$$\frac{dZ}{dt} = \frac{\partial Z}{\partial t} + u\frac{\partial Z}{\partial x} + v\frac{\partial Z}{\partial y} \qquad (2)$$

One of the simplest forecasting methods is to set the local rate of change $(\partial Z/\partial t)$ to zero. This is equivalent to keeping the most recent observation frozen and taking it as the prediction. This approach is usually termed as Eulerian persistence and can be expressed as

$$\hat{Z}(t_0 + \tau, x, y) = Z(t_o, x, y) \qquad (3)$$

where Z is the observed reflectivity field, t_0 is the start time of the forecast, τ is the lead time, and $\hat{Z}(t_0 + \tau, xy)$ is the forecasted reflectivity at time $t_0 + \tau$ and position (x, y).

Another popular forecasting approach, called Lagrangian persistence, is to set the source-sink term to zero

$$0 = \frac{\partial Z}{\partial t} + u\frac{\partial Z}{\partial x} + v\frac{\partial Z}{\partial y} \qquad (4)$$

and advect Z following the motion of precitation parcels. Therefore, for a displacement vector $(\Delta x, \Delta y)$, a forecast is generated using

$$\hat{Z}(t_0 + \tau, xy) = Z(t_o, x - \Delta x, y - \Delta y) \qquad (5)$$

Lagrangian persistence can be extended by introducing a source-sink term $S_Z = dZ/dt$, which allows for growth and dissipation of precipitation. Then Eq. (5) becomes

$$\hat{Z}(t_0 + \tau, x, y) = Z(t_o, x, y - \alpha) + S_Z(t_o, x, y - \alpha) \qquad (6)$$

In this study Lagrangian persistence with no source-sink term has been employed as the main forecasting technique and Eulerian peristence has been used as the reference forecast with which the skill of the Lagrangian persistence is compared. Therefore Eq. (5) is the general equation of the forecasting technique used here.

2.2 Advection vector estimation

The first step in the forecasting procedure is the estimation of the advection vectors which describe the storm motion. Two different methods were used to generate global (spatially uniform) and spatially distributed vectors. The global advection vector estimation is based on a well known maximum cross-correlation technique (Li et al., 1995). The technique starts by taking the first map from two successive maps and extracting a rectangular domain for which advection velocity and direction is to be determined. Then the two dimensional array constituting this domain is horizontally shifted in all directions within a given radius and compared with the corresponding array from the consecutive map. The comparison is made by computing the correlation coefficient between each array-pair. Finally the location of the array in the second map for which the correlation is maximum is selected as the endpoint of the translation vector.

Though the cross-correlation technique is robust and relatively accurate, it becomes computationally intensive when applied for estimating spatially distributed vectors. The estimation of distributed vectors is based on the optical flow algorithm developed by Farnebäck (2003). In computer vision, optical flow is one of the standard techniques used for motion vector estimation from two subsequent images. At the heart of optical flow methods is Eq. (4), which is commonly referred to as the optical flow equation in computer science. The underlying idea is to explain the discrete temporal ($\Delta Z/\Delta t$) and spatial derivatives ($\Delta Z/\Delta x$ and $\Delta Z/\Delta y$) with a continuous motion field. It is assumed that that precipitation objects remain constant in intensity and only change in shape: $dZ/dt = 0$. dZ/dt is seen in the coordinates of the flowing data (Lagrangian framework). This implies that all changes in intensity are explained by motion. Then the only two unknowns in Eq. (4), u and v, are solved for using additional constraining equations. Although the constant intensity assumption is not strictly obeyed by precipitation, previous application of optical flow algorithms have produced sensible flow patterns that resemble the actual motion of precipitation well (Bowler et al. 2004, Pfaff and Bárdossy 2011).

2.3 Advection of radar reflectivity

After the advection vector field has been estimated an advection scheme is used to calculate the forecasts at different lead times. When using global advection vector, all the pixels in the observed image are displaced equally over the forecast interval. This results in a moving precipitation field that preserves its spatial pattern since translation is applied equally to each pixel. While the use of a single advection vector is a gross approximation for forecasting at synoptic scales, it is still a useful approach when working on domains with limited spatial extent, such as the coverage of a single radar. For the advection with distributed vectors, a forward scheme is used where each pixel is assigned a displacement vector which is kept constant over the entire forecast period. In other words, the displacement vector is advected together with the precipitation. When the displacement vector assigned to a given pixel is a non-integer number of pixels (spatial resolution of the image) per time step, an advected precipitation pixel will not be aligned with the pixel borders. The value from such a pixel is redistributed to the neighbouring pixels according to the proportion of the intersecting area. The forward scheme has the advantage of being mass conservative. In addition, embedded features may be appropriately advected since the scheme allows independent advection of two area of precipitation (Bowler et al. 2004).

2.4 Growth and dissipation of precipitation

The source-sink term in Eq. (6) has been set to zero and Eq. (5) is used as the main equation in the forecasting technique investigated here. The persistence of growth or dissipation of precipitation is low for convection at the storm-scale and other factors such as daytime and synoptic forcing may dominate over advection. While radar precipitation accumulation procedures have benefited from the interpolation of intensities between successive radar observations, extrapolating changes in intensity and size have yielded little if any improvement to forecasting procedures at the storm-scale (Tsonis and Austin 1981; Wilson et al. 1998).

## 2.5 Choice of reflectivity as the variable for the analysis

Eqs. (1)-(6) may be formulated in terms of precipitation rate (R) as well. In fact, the main variable of interest when applying precipitation forecasting for flood warning is precipitation rate. However, it was decided to use logarithmic reflectivity ($dBZ = 10logZ$) throughout this study because of the following reasons:

- If the advection vector estimation is applied to linear R or linear Z, the motion of a few pixels with high intensity will dominate the result. The differential motion of such pixels can be chaotic with very low persistence. The advection vectors resulting from such motion might improve only the forecasts for the shortest lead time while spoiling the forecasts beyond the shortest lead time. The use of logarithmic scale significantly reduces this influence from high intensity pixels.
- Both the maximum cross-correlation and optical flow methods generally perform better on images with smoother variation in intensity (lower intensity gradients). dBZ images are smoother than images of linear Z or R.
- The uncertainties in $Z - R$ relationships used for converting Z to R may introduce erroneous spatial patterns of precipitation. A very good example where this is especially true is when one uses spatially constant $Z - R$ parameters for inhomogeneous precipitation field with both stratiform and convective precipitation.
- The evaluation of the forecasts can be made by comparing them with observed reflectivity fields and not precipitation rates on the ground (Section 4).
- In the context of forecasting, relative errors are of more importance than absolute errors. An error of, for instance, 4 mm/hr is large for a forecasted value of 5mm/hr while it is insignificant for values beyond 50 mm/hr. Working in logarithmic domain is one way of considering relative errors.
- And finally, reflectivity is the quantity directly measured by the radar.

3 Setup of the experiment

3.1 Prediction domain

The prediction domain used in this study is a 200x200 km rectangular area centred on the Rissa radar (Figure 1). Ideally, the prediction domain should be limited to the boundary of the Trondheim municipality or even the region in the municipality which is prone to flooding. However, the type of events which are of interest here have limited spatial extent and move relatively fast. Combined with the 15min scanning interval of the Rissa radar, this will give too little data to work with. The extension of the prediction domain to the 200x200 km box gives sufficient data to carry out evaluation of forecasts even when considering a few separated events as has been done in this study. It is assumed that the precipitation occurring outside Trondheim has the same probability of occurring inside Trondheim as well. The upped limit of the extent of the prediction domain is dependent on the longest lead time and the average velocity of the storm to forecast.
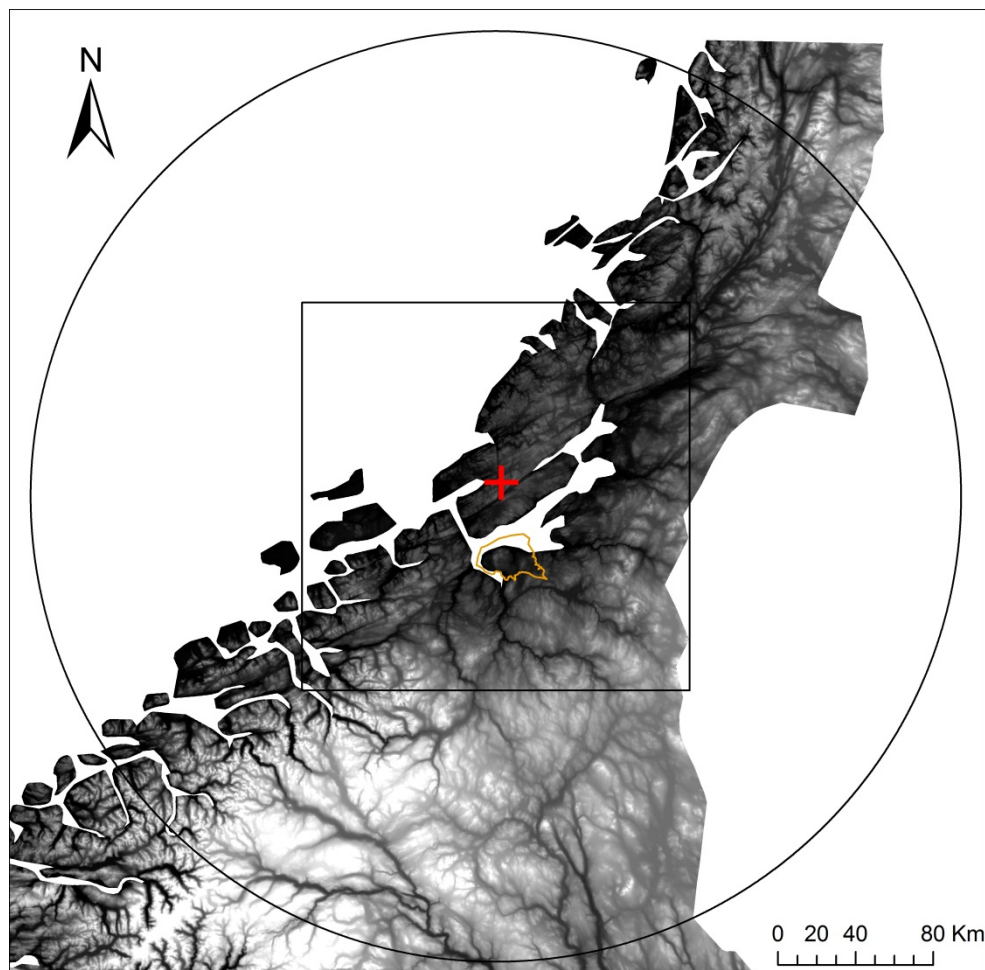
Figure 1. *Map showing the location of Rissa radar (red cross), administrative boundary of Trondheim municipality (yellow polygon), extent of the prediction domain (square box) and the maximum radar coverage (circle).*

3.2 Data

Radar reflectivity data from the Rissa Radar were obtained from the Norwegian Meteorologic Institute (MET) for use in this study. The radar is located in Olsøyheia in the municipality of Rissa and is situated at an elevation of 616m above sea level. It is a C-band Doppler radar with a half-power beam width of 1 degree. The raw radar data obtained consist of volume scans of radar reflectivity collected in polar coordinates in the form of plan position indicators (PPIs). Stationary echoes in the lowest PPIs are removed during data acquisition by using a Doppler filter. The temporal resolution of the radar data is 15min. The azimuthal and radial resolutions of the lowest PPI used are 1degree and 250m respectively. The polar reflectivity maps were projected to the ground level assuming standard atmospheric refraction of the radar beam and converted to cartesian maps with 1x1 km resolution through area-weighted interpolation. These cartesian reflectivity maps are used both as input to the forecasting procedure and for evaluating the forecasts. For the analysis in this study, a lower reflectivity threshold of 7dBZ is used. This corresponds to a precipitation rate of 0.1mm/hr using Marshall-Palmer Z-R relation with parameters $a = 200$ and $b = 1.6$ (Marshall and Palmer 1948). Pixels with measurements below this threshold are considered as "no precipitation" pixels.

The reflectivity data has not been corrected for errors due to the vertical profile of reflectivity, visibility, attenuation and others. This reduces the quality of the data in terms of quantitative precipitation estimation. But the significance of these errors is much less in the context of short-term forecasting for flood warning purposes in urban areas. It is the exceedances over given thresholds which are important and not the precise quantities in the forecasts. One type of error which cannot be neglected is the contamination by ground clutter. The residual clutter remaining after doppler-filtering will directly affect the advection vector estimation and spoil the forecasts. In order to avoid this, a clutter mask was generated using a combination of a static map with simulated clutter and a map with pixels with too high frequency of occurrence. The pixels falling within this mask were excluded from the entire process.

Rainfall measurements on the ground were available from six tipping-bucket rain gauges situated in Trondheim. These measurements were used to calculate return periods of the candidate events which passed over Trondheim.

3.3 Selected events

Two events which occurred on 13 August 2013 and 28 June 2010 were selected for the analysis based on the following criteria:

- The event should have passed over Trondheim.
- The return period should be at least 20 years as calculated from ground observations in Trondheim.
- The event should contain convective elements either as embedded convection or as isolated cells.
- There should not be significant portions of two separate events coexisting in the prediction domain at the same time.

The characteristics of each event are summarized in Table 1. The event of 28 June 2010 was selected even if it had a return period of 2 years since the proportion of its precipitation are with high intensity was equivalent to that of the 13 August 2007 event. The event of 13 August 2007 caused overloading of the urban drainage system and the resulting flood caused large damages (Risholt 2009; Thorolfsson et al. 2008). The beginning of each event is defined as the first time step when a part of the precipitation envelop entered the prediction domain and the end is defined as the time step just before it cleared out of the domain. The synoptic situations during the two events are shown in Figure 2 and Figure 3. Both events are associated with the passage of a trough. The time series of radar images scanned during the passage of the storms are shown in Figure 4 and Figure 5.

Table 1. *Statistics of the two events used in this study. The extent is defined as the precipitation area falling inside the 100x100km prediction domain and with precipitation rates higher than 7dBZ (0.1mm/hr). The last four columns give the fraction of that area with rates higher than the indicated reflectivity values (precipitation rates). The fractions are averages over the entire period. For instance, the proportion of the area with reflectivity values (precipitation rates) higher than 40dBZ (11.5mm/hr) over the 6-hr duration of the August 2007 event was 2.4%.*

Date	Start (UTC)	Duration (hr)	Return period (yr)	Extent (10^3 km^2)	>25dBZ (1.3mm/hr) (%)	>30dBZ (2.7mm/hr) (%)	>35dBZ (5.6mm/hr) (%)	>40dBZ (11.5mm/hr) (%)
13 Aug 2007	15:30	6	>100	7.5	37	22	9.0	2.4
28 Jun 2010	14:15	7	2	8.5	45	29	12	2.4
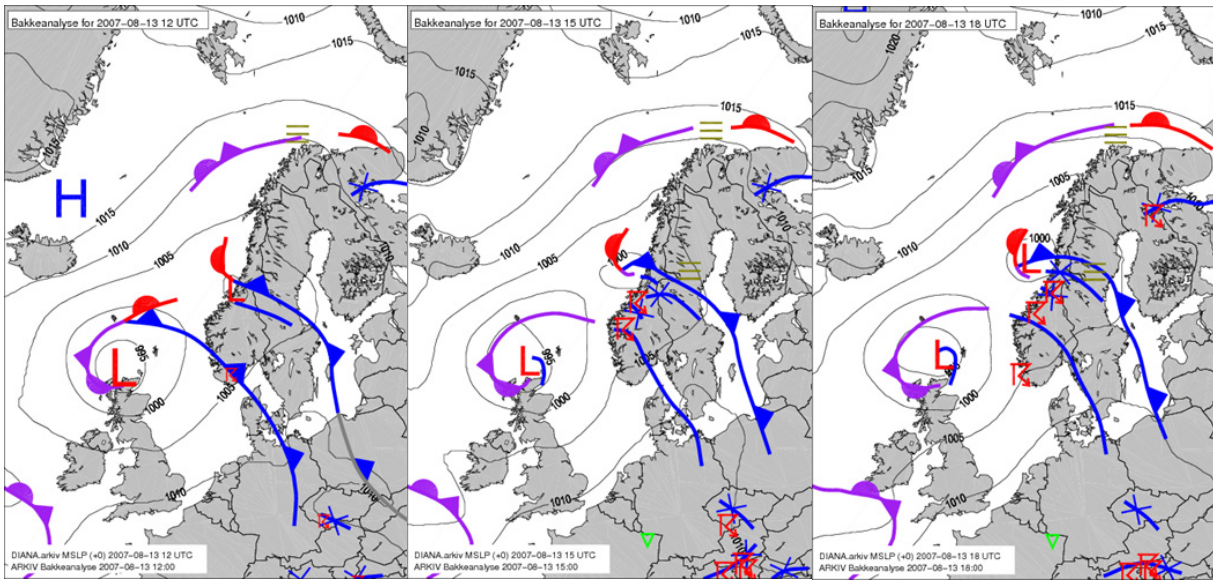
Figure 2. *Synoptic situation during the event of 13 August 2007 (Source: MET).*

PROJECT NO.
12X846

REPORT NO.
TR A7379

VERSION
1

12 of 33
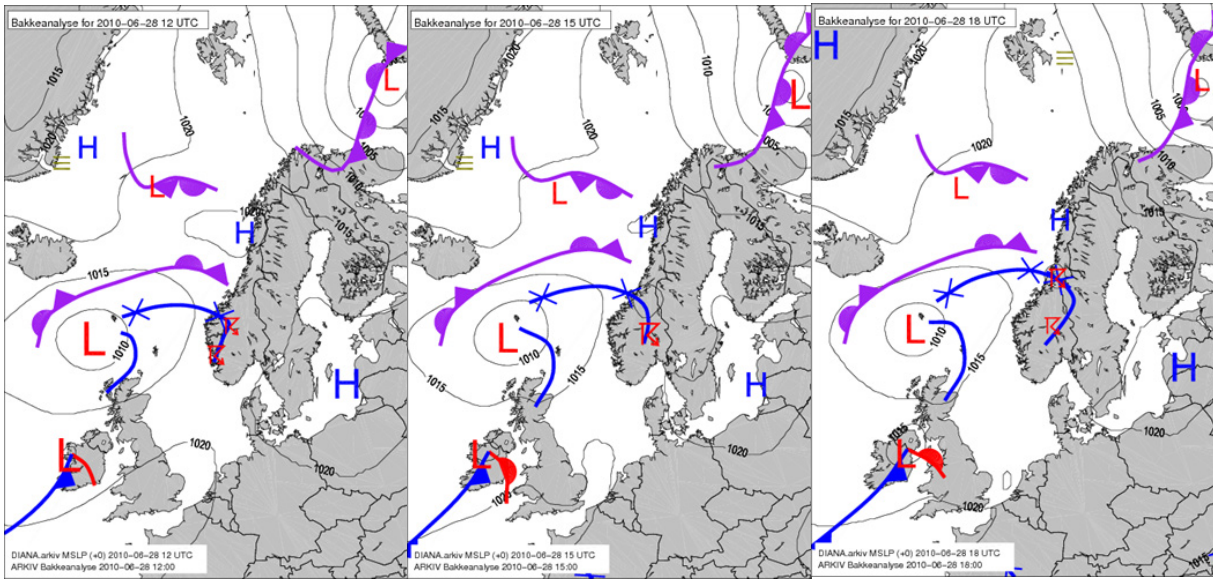
Figure 3. *Synoptic situation during the event of 28 June 2010 (Source: MET).*
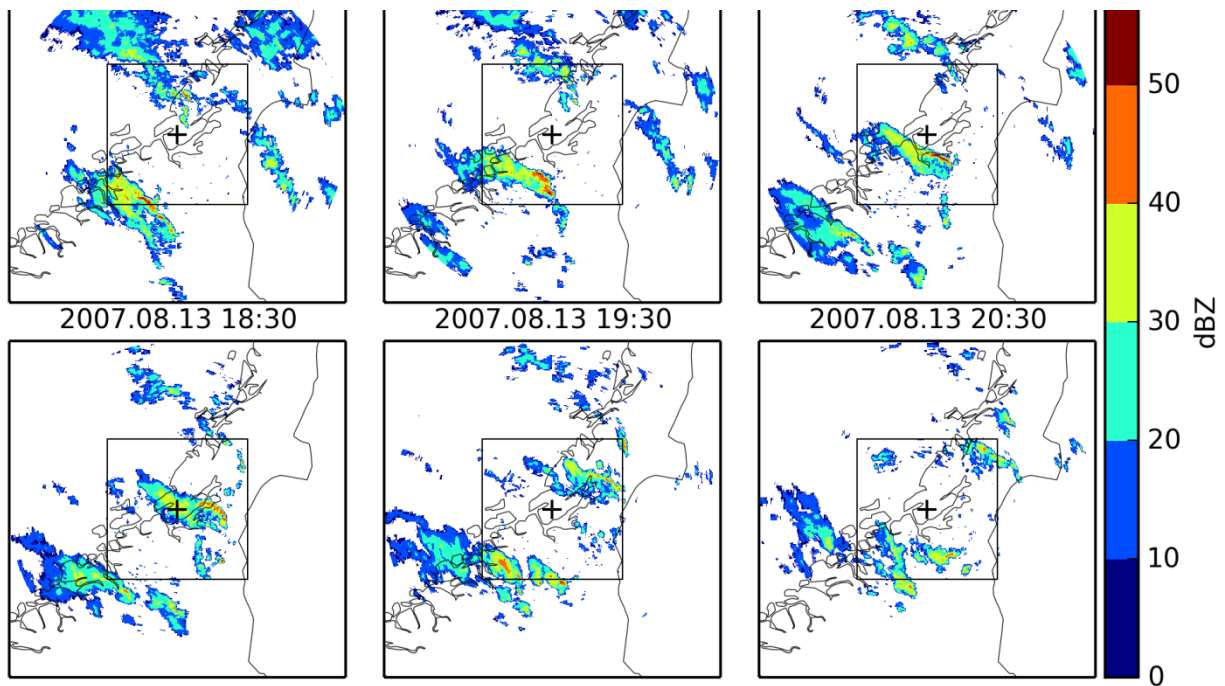
Figure 4. *A time series of radar images at 1 hour interval for the event of 13 August 2007.*
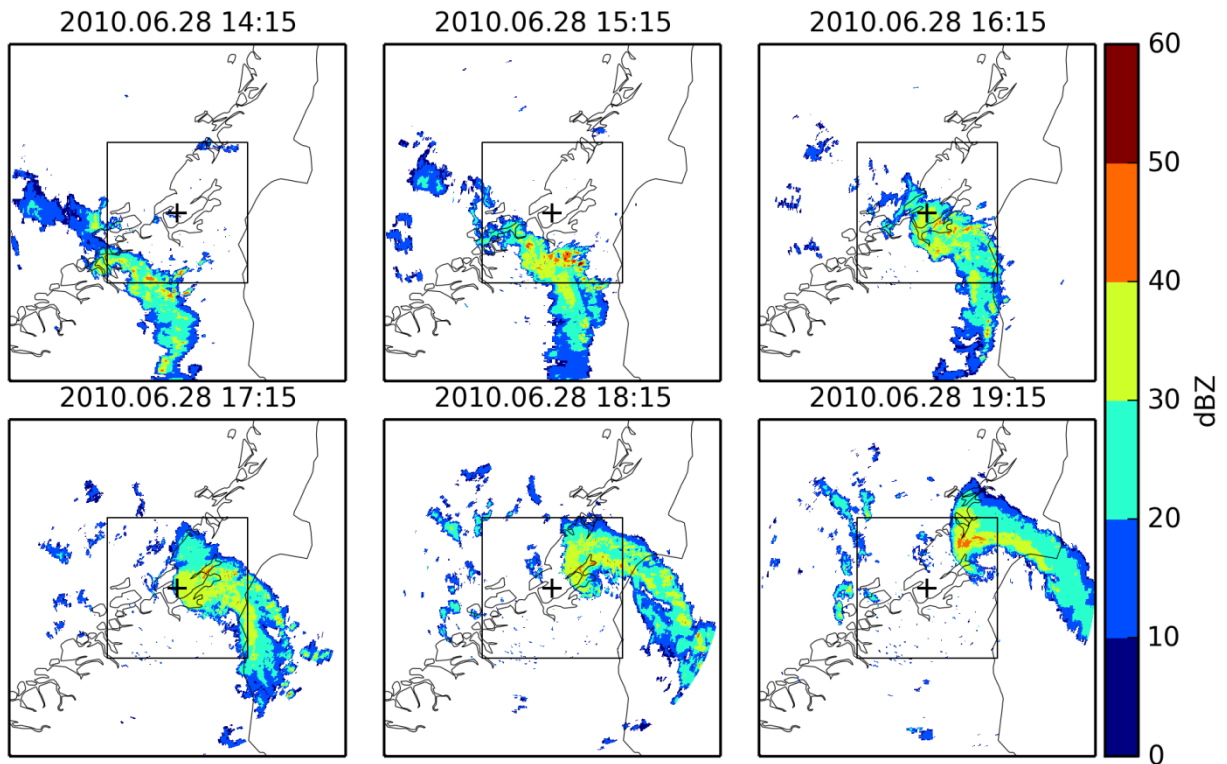
Figure 5. *A time series of radar images at 1 hour interval for the event of 28 June 2010.*

3.4 Summary of the steps in the experiment

The following steps were carried out for each selected event:
1. Determine the advection vector field between successive reflectivity images
2. Generate forecasts for lead time of up to 2hours with 15min interval by advecting the radar reflectivity using the global advection vector.
3. Repeat step 2 using Eulerian persistence as the forecasting model
4. Calculate performance measures by comparing the forecasted and observed radar images
5. Repeat step 4 for higher reflectivity thresholds (25, 30, 35 and 40dBZ) and larger verification areas (3x3, 5x5, 7x7, 9x9 and 11x11 km) to analyse the scale dependence of predictability

4 Evaluation criteria

The following six performance measures were used to evaluate the forecasting procedure: correlation coefficient (CORR), probability of detection (POD), false alarm ratio (FAR), critical success index (CSI), equitable threat score (ETS) and the conditional mean absolute error (CMAE). They measure the agreement between the forecasts (F) and the observations (O) based on a pixel-to-pixel comparison. The correlation coefficient CORR is defined as:

$$CORR = \frac{\sum_{i=1}^{N}(O_i - \bar{O})(F_i - \bar{F})}{\left(\sum_{i=1}^{N}(O_i - \bar{O})^2\right)^{0.5}\left(\sum_{i=1}^{N}(F_i - \bar{F})^2\right)^{0.5}} \tag{7}$$

where the bar represents the spatial average values and N is the number of pixels in the prediction domain. The correlation coefficient is not a sufficient measure of agreement since it is not sensitive to proportional differences between the observation and forecasts.

POD, FAR, ETS and CSI are categorical scores which describe the skill of predicting the occurrence of precipitation above a given threshold. They are based on a 2 x 2 contingency table as given in Table 2 and are defined as follows:

$$POD = \frac{hits}{hits + misses} \tag{8}$$

$$FAR = \frac{false\ alarms}{hits + false\ alarms} \tag{9}$$

$$CSI = \frac{hits}{hits + misses + false\ alarms} \tag{10}$$

and

$$ETS = \frac{hits - hits_{random}}{hits + misses + false\ alarms - hits_{random}} \tag{11}$$

$$where\ hits_{random} = \frac{(hits+misses)(hits+false\ alarms)}{hits+misses+false\ alarms+correct\ negatives} \tag{12}$$

Table 2. *A general 2x2 contingency table used in the calculation of skill scores for a given threshold value T.*

		Forecasts	
		F > T	F <= T
Observations	O > T	Hits	Misses
	O <= T	False alarms	Correct negatives

The CSI, also known as threat score, ranges from 0 to 1 where 0 indicates no skill and 1 is a perfect score. It measures the fraction of the observed and/or forecasted precipitation that was correctly predicted. Unlike the POD and the FAR, it takes into account both false alarms and misses, and is therefore a more balanced score. The ETS, also known as Gilbert skill score, is similar to CSI but accounts for hits associated with random chance. It ranges from -1/3 to 1 where 0 indicates no skill and 1 is a perfect score.

Neither the correlation coefficient nor the categorical skill scores provide a direct measure of how accurate the forecasted quantities are. This is the main reason for including the conditional mean absolute error (CMAE) which is defined as follows:

$$CMAE = \frac{1}{hits} \sum_{i=1}^{hits} |O_i - F_i| \tag{13}$$

Owing to the nature of the Z-R relation, CMAE value in logarithmic reflectivity can be expressed as a factor in terms of linear precipitation rates. Therefore, CMAE in dBZ corresponds to a relative error in mm/hr. For example, for an exponent of 1.6 in the Z-R relation (Marshall and Palmer 1948), a CMAE of 9.5dBZ corresponds to a factor of 4 for precipitation rates. As CMAE is computed over only the hits and not the entire domain, it should be combined with POD values. A POD of 40% and CMAE of 9.5dBZ indicate that the occurrence of precipitation has been correctly predicted for 40% of the precipitation area and that the average error for this area is a factor of 4 in terms of precipitation rates.

Not all the performance measures described here have been referred to in the discussions (Section 5). The motivation behind presenting all the performance measures in the results is to give a fuller picture of the performance to readers with different perspectives.

5 Results and discussions

5.1 Predictability of precipitation

The performance measures computed for the event of 13 August 2007 and 28 June 2010 are shown in Figure 6 and Figure 7 respectively. A degradation of performance with lead time is obvious from the figures and is expected. The Lagrangian persistence model performs significantly better than the simple Eulerian persistence for both events. This indicates that advection is a very important factor for successfully predicting the events. The comparison between the performance measures of the two events (Figure 8) shows that the event of 28 June 2010 has better predictability. This difference in predictability can be attributed to the difference in the rates at which the precipitation patterns in the two cases evolve with time. The event of 13 August 2007 had faster temporal evolution with its precipitation envelop significantly deforming in shape between the 15 min scanning interval and its convective region showing differential motion. The effect of this evolution was also evident from the global advection vector estimation results where the average of the maximum cross-correlation between successive images was lower for the event of 13 August 2007. This result is in line with the general finding in previous studies that storms with smaller spatial scale have less predictability than large scale storms (German and Zawadski 2002; Turner et al. 2004). The event of 28 June 2010 had a much larger spatial extent (Figure 5).
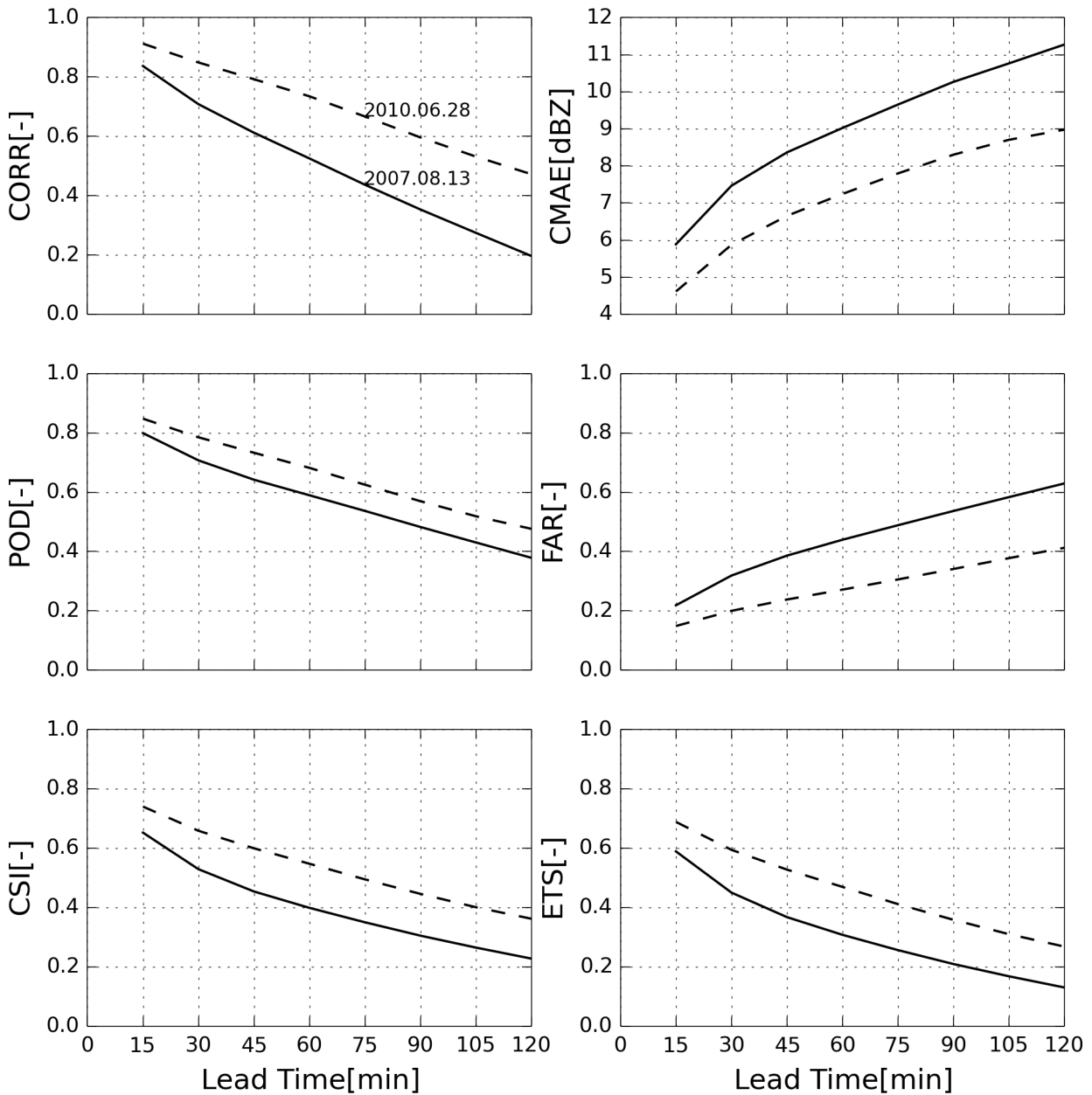
Assigning an absolute number to the predictability of a single event is difficult since this depends on the performance measure used, how it was calculated and what is considered acceptable or important by the user of the forecasts. In order to fairly compare results from different studies, the conditions under which the studies were carried out should be similar. These include, among others, type of precipitation events considered, extent of the prediction domain, spatial resolution of the forecasts, type of variable used (reflectivity or precipitation rate) and minimum threshold used to define 'no precipitation' pixels. One predictability measure used in previous studies (Zawaski et al. 1994; Grecu and Krajewski 2000) is the decorrelation time; defined arbitrarily as the moment the correlation becomes less than 0.5. Using the same definition here, the predictability of the 13 August 2007 event becomes slightly over one hour while that of the 28 June 2010 event extends up to almost two hours. The CSI can also be a useful reference as the measure of predictability since it is a score frequently used in large forecast evaluation projects (Ebert et al 2004, Wang et al. 2009; Wilson et al. 2010). CSI values obtained for the two events generally indicate good predictability when compared with values obtained in other studies (Berenguer et al. 2011) for similar type of events.
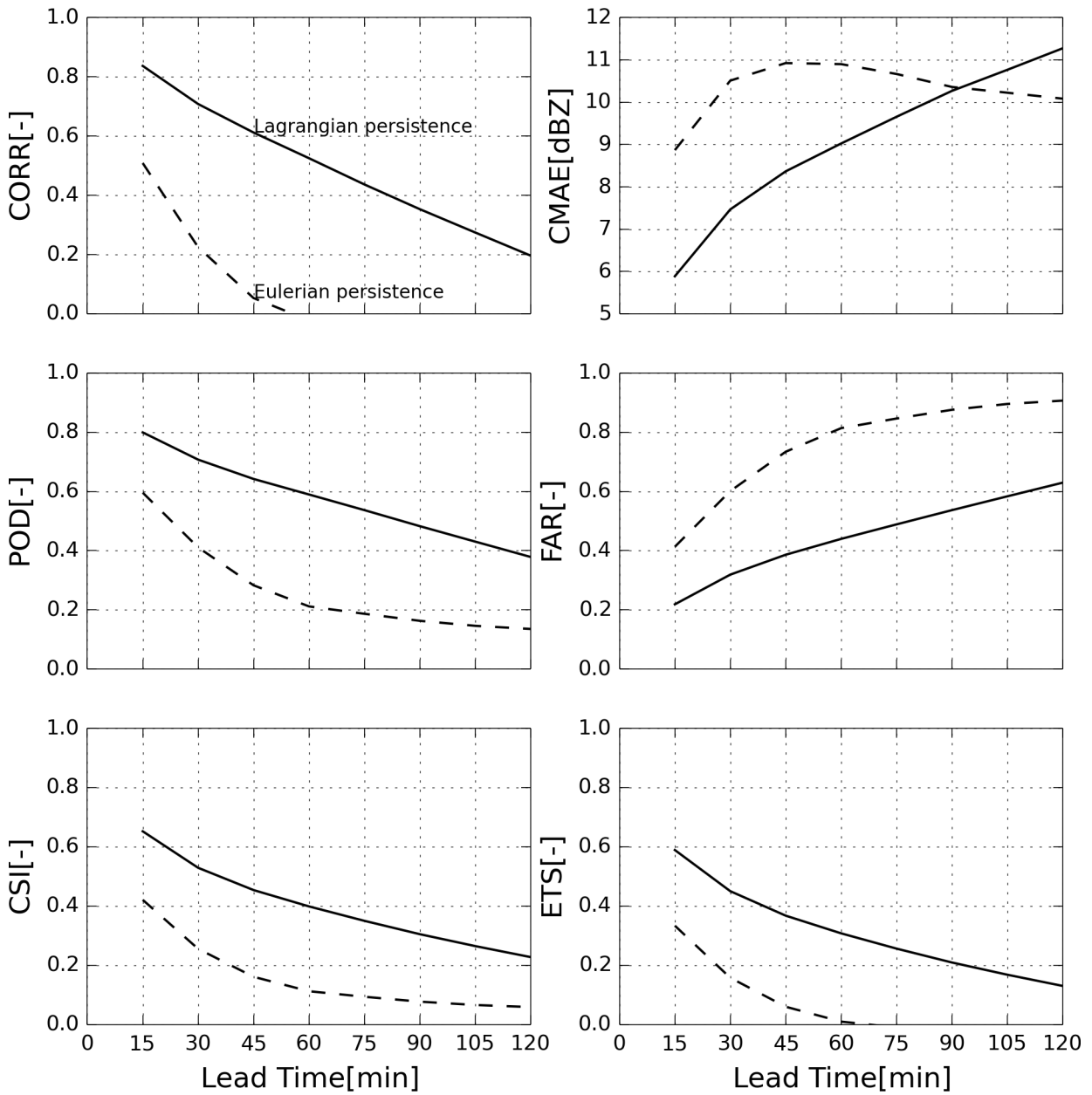
Figure 6. *Performance measures calculated for the event of 13 August 2007.*

PROJECT NO.
12X846

REPORT NO.
TR A7379

VERSION
1

18 of 33
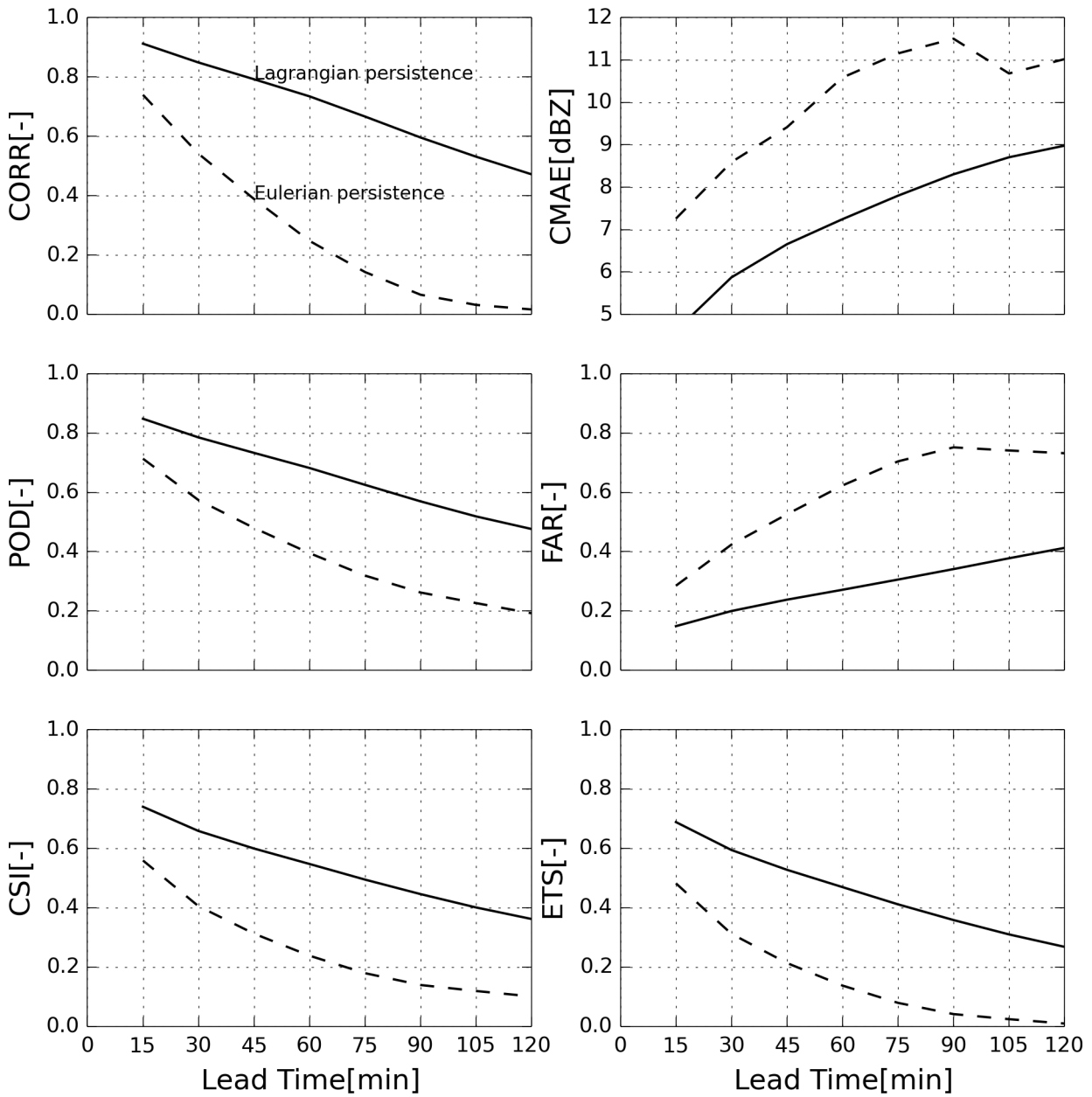
Figure 7. *Performance measures calculated for the event of 28 June 2010.*

PROJECT NO.
12X846

REPORT NO.
TR A7379

VERSION
1

19 of 33

Figure 8. *Performance measures calculated for the two selected events.*

## 5.2 Scale dependence of predictability

The results presented in the previous section are all based on a single reflectivity threshold of 7dBZ, which is used as the minimum reflectivity below which pixels are considered as 'no precipitation'. While these results indicate the predictability of the storm envelope, they do not give information on the scale dependence of predictability. A simple method of scale decomposition is to convert the observations and forecasts into 'precipitation' and 'no-precipitation' binary maps using various intensity thresholds and then compare these maps using the categorical skill scores described in section 4 (German and Zawadski 2002, Van Horne et al. 2006). This is possible due to the intensity-size relationship evident in precipitation fields. Following this

PROJECT NO.
12X846

REPORT NO.
TR A7379

VERSION
1

20 of 33

method, the CSI was calculated for four reflectivity thresholds higher than the 'no precipitation' threshold (Figure 9). These are 25, 30, 35 and 40dBZ corresponding to1.3, 2.7, 5.6 and 11.5 mm/hr respectively according to the Marshall Palmer Z-R relation (Marshall and Palmer 1948). The CSI was chosen here due to its wide application and because it synthesizes the information contained in POD and FAR.

The plots in Figure 9 clearly reveal the effect of intensity threshold on the forecasting skill for the two events. The forecast skill decreases for both events as the threshold gets higher. A reduction in CSI for higher intensities and small scale features had been reported in previous studies. In the Beijing 2008 Olympics' Forecast Demonstration Project, where eight nowcasting systems participated, Wang et al. (2009) showed that the maximum CSI for forecasts of hourly precipitation accumulation greater than 1 mm/h increased from 0.2 in 2000 to 0.45 in 2008, although the maximum CSI for rain greater than 10 mm/h was still only 0.15. Berenguer et al. (2011) report a CSI for 60 minute forecasts of reflectivity (dBZ) at 1 km resolution of approximately 0.5 for widespread rainfall, and in the range of 0.1 to 0.3 for isolated convection. Lee et al. (2009) found that the CSI decreased with increasing rain rate and forecast lead time: the CSI for 60 minute rainfall forecasts decreased from 0.60 for 0.1 mm/h to 0.2 for 10 mm/h rain rates. Ebert et al. (2004) reported that the CSI for rain greater than 20 mm/h is essentially zero. Precipitation features at scales of few kilometres typically evolve relatively faster, have shorter lifetimes and show differential motion. Such features significantly contribute to the decorrelation of Lagrangian persistence. Unfortunately, the type of precipitation which is of interest in urban flooding, convective precipitation, is exhibits one or all of the above characteristics. Considering the typical intensities of convective precipitation, this implies that more intense features in a precipitation field are typically of small spatial scale and thus less predictable.

Another factor which adds to the overall reduction of CSI values in this study is the high spatial resolution of the forecasts. The calculation of all the performance measures is based on pixel-to-pixel comparisons at the resolution of 1 km. The results in stricter evaluation with lower tolerance to errors made due to misplacement of predicted features. If a forecast at pixel level does not compare well with the available observation, it does not mean that the performance is poor. This is why some studies employ other evaluation methods, such as object-based methods, in addition the pixel-to-pixel verification (Zahraei et al. 2012). In order to analyse the effect of increasing tolerance to error due to misplacement, the CSI was calculated for an extended verification area surrounding a forecasted pixel. The verification areas are square regions with side lengths ranging from 3 to 11 pixels. When evaluation over an extended grid, each individual pixel is compared against all of the pixels located in the square region surrounding that pixel. For example, a 'hit' is registered if the forecast at the pixel of interest and the observation in one of the surrounding pixels both exceed the specified threshold. Such an approach had been used by Van Horne et al. (2006).

The results of the performance for larger verification area are presented in Figure 10 and Figure 11 for the 13 August 2007 and 28 June 2010 events respectively. Both figures illustrate the increase in forecast skill, as quantified by the CSI, as the verification area is increased from a single pixel (1 km^2) up to an 11 x 11 pixel region (121 km^2). CSI values for the smallest verification area correspond to the results shown in Figure9. Though the forecast skill improves for both events, the rate of improvement varies between the events. This suggests that errors due to misplacements are dependent on storm structure and scale. While there are improvements in forecast skill score at all reflectivity thresholds, the improvements are greater for higher thresholds in the case of both events. This is likely due to the fact that features which are smaller than the size of the verification area are usually intense features with higher probability for misplacement. It can also be observed that the rate of improvement reduces with lead time. This is probably due to the initiation of new features occurring after the time of forecast, the death of features observed at the time of forecast or the fast temporal evolution of existing features in the precipitation field. Increasing the verification area does not have an effect in such cases since Lagrangian persistence with a global advection vector involves the translation of a frozen precipitation field.
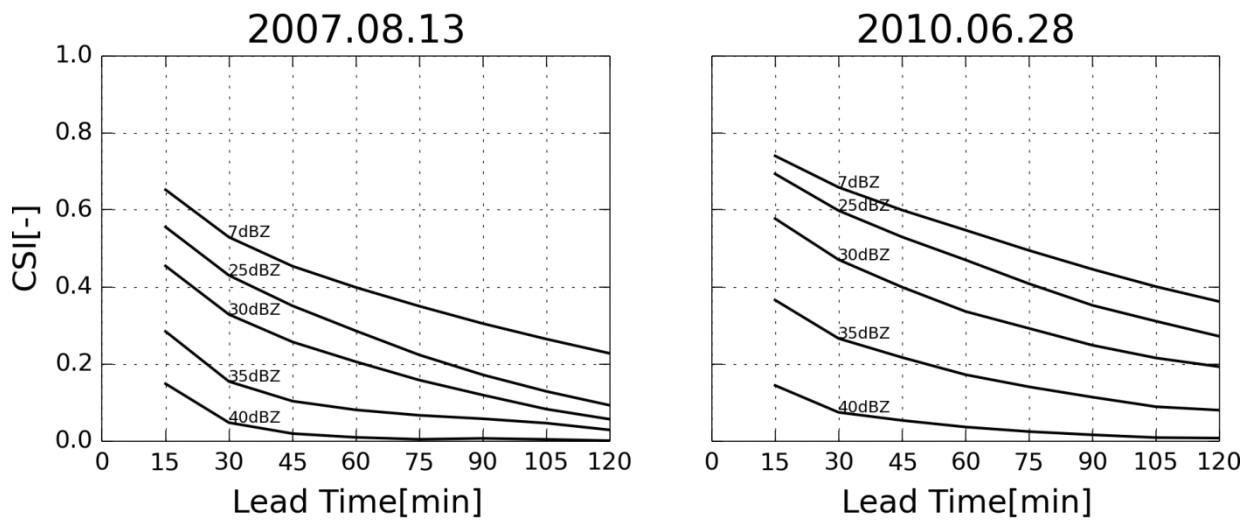
Figure 9. *CSI at several reflectivity thresholds versus forecast lead time for the two events.*
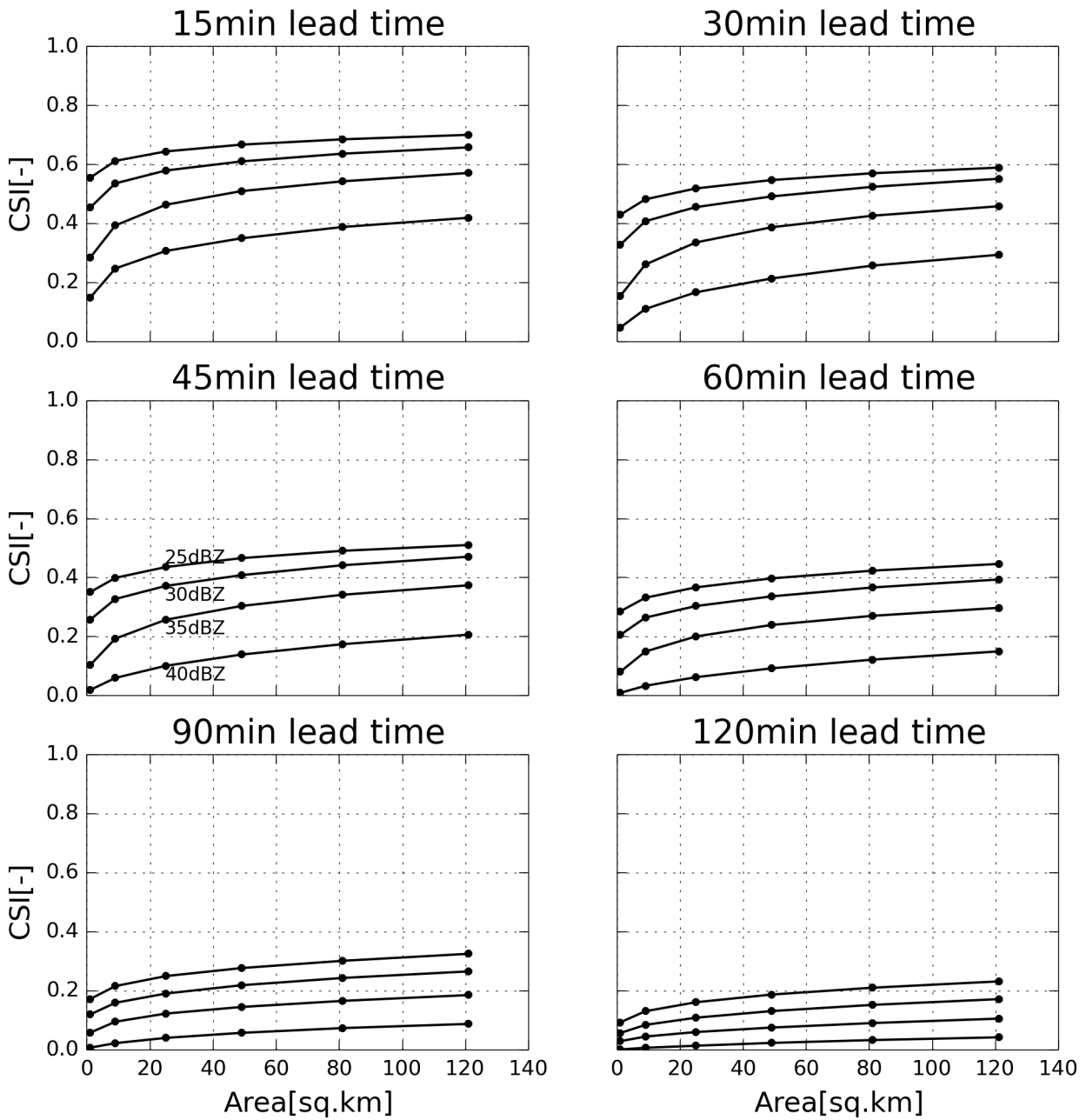
Figure 10. *CSI at several reflectivity thresholds versus forecast verification area for the event of 13 August 2007.*
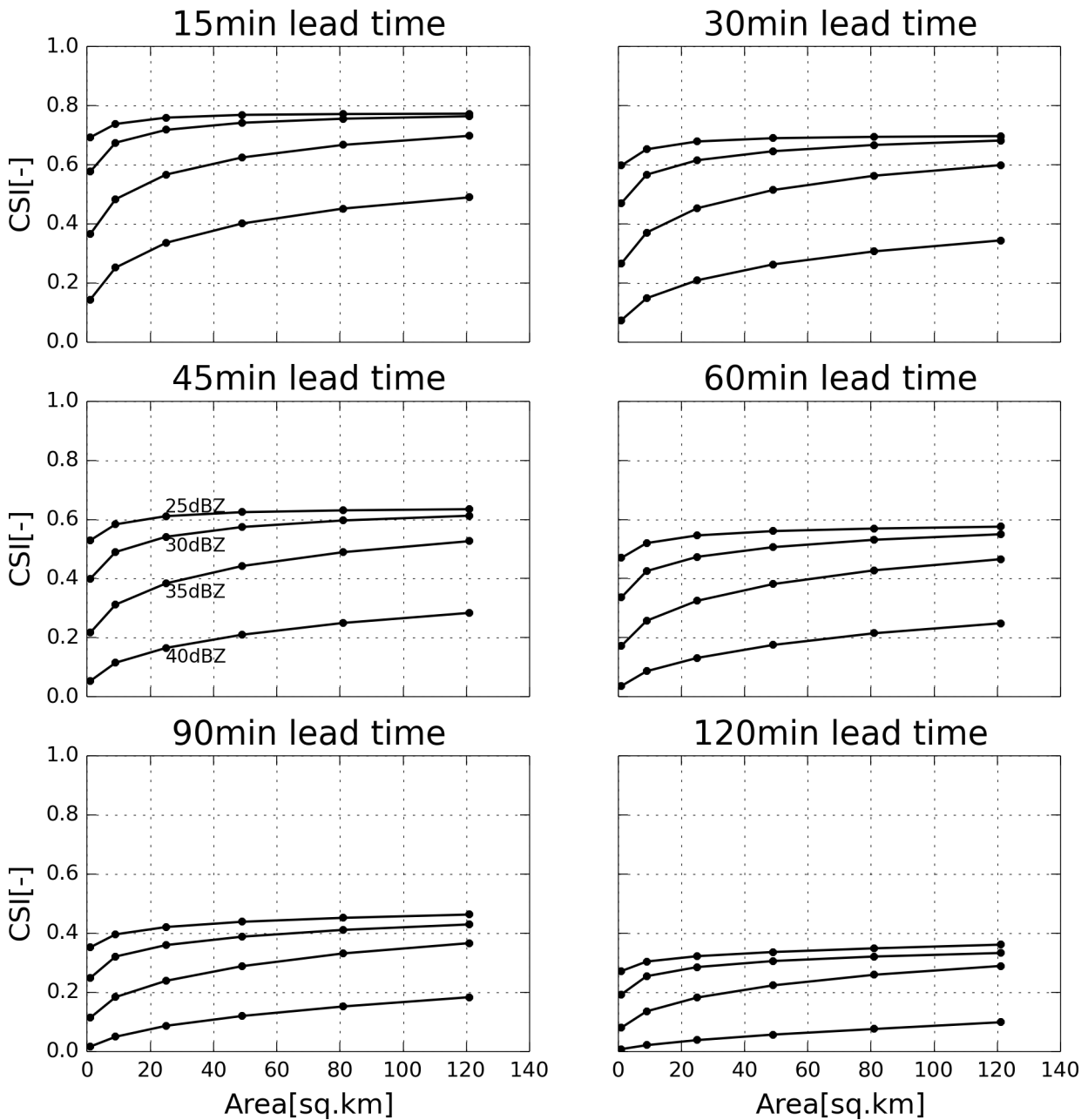
Figure 11. *CSI at several reflectivity thresholds versus forecast verification area for the event of 28 June 2010.*

5.3 Representativeness of a global advection vector

The forecasts evaluated in this study were generated using a global advection vector. This assumption of spatially uniform advection introduces errors in the forecasts when there are changes in the relative location of storm features. Various studies have documented that differential motions exist within a storm and are commonly observed in the case of embedded convective cells (Bellon and Zawadski 1994; German and Zawadski 2002). Both the events analysed in this study have convective features either as embedded cells or

with a trailing stratiform region. Figure 12 presents an example from the event of 13 August 2007 where differential motion of convective features has resulted in erroneous forecasts at longer lead times. It can be observed that the convective region has been misplaced for lead times beyond 60min. At a first glance, it seems that the whole precipitation area should have been advected more to the east. This implies a wrong global advection vector. However, a closer look at the time series of observed images revealed that the global advection vector estimated before each forecast was representative of the motion of the majority of the pixels. The change in morphology of the main storm envelop makes it difficult to see this representativeness from the eight images in Figure 12. But it can be easily observed that the smaller features south of the main storm envelop have been forecasted to the same location for all the lead times. The ellipse marked at the same position in all the images encloses these features in all the forecasts for all lead times. The main reason for the failure of forecasting the position of the convective region at the longer lead times is that this region actually had a larger advection component to the east than was indicated by the global advection vector. This difference is shown in Figure 13 where both the global and distributed advection vectors have been plotted over two successive observed images. The distributed advection vector estimation shows how the motion direction of the convection region deviates towards the east as compared to the global vector which shows very little advection component to the east.

The results (not presented here) from the few attempts made in this study to use the distributed vectors in the forecasting of the 13 August 2007 event revealed a shortcoming of the forward advection scheme described in Section 2.3. In this scheme the vector obtained for each pixel is kept constant throughout the forecast period when advecting the precipitation from that pixel. For advection vectors which point away from each other, as the ones shown in Figure 13, this results in unrealistic divergence of the storm area at longer lead times. This divergence creates a 'banded' structure in the forecasted field. And it also results in intensification of intensity in the case of converging vectors. Therefore, a backward advection scheme as described by German and Zawaski (2002) may be a better approach.

It is not always the case that using spatially distributed advection vectors will yield better forecasts. The small scale features inside a storm may have differential advection velocities. Combined with the growth and decay process within the storm, such features may have shorter predictability. The storm envelop, on the other hand, usually has a higher degree of predictability as the envelop motion will remain relatively stable over longer lead times. In such situations, it is advantageous to not let the motions of the small features affect the forecasts for lead times which are beyond the lifetime of these features. In view of this, various techniques have been proposed for smoothing the precipitation field to separate or filter out the small and perishable features from the large-scale motion (Seed 2003). The event of 28 June 2010 had several dynamic small scale features within the storm while the large scale feature had relatively higher degree of predictability. The forecasts for this event were not significantly affected by the differential motions of the small scale features since the maximum cross-correlation method of estimating global vector is not sensitive to the presence of such features. Samples from the forecasts of this event are shown in Figure 14. The position of the storm envelop has been well predicted. In Figure 15 both the global and distributed advection vectors have been plotted over two successive observed images from this event.
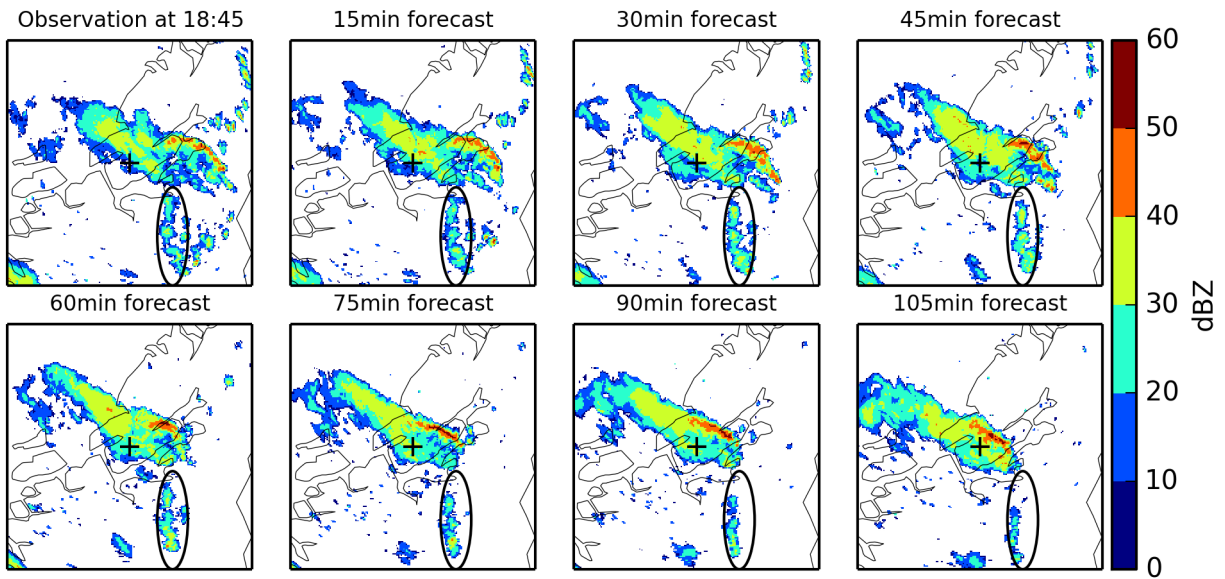
Figure 12. *Observed radar image for 13 August 2007 18:45 and forecasted images generated for the same time at different lead times. For a perfect forecast all the images should be identical. The ellipse is located at the same position in all the images.*
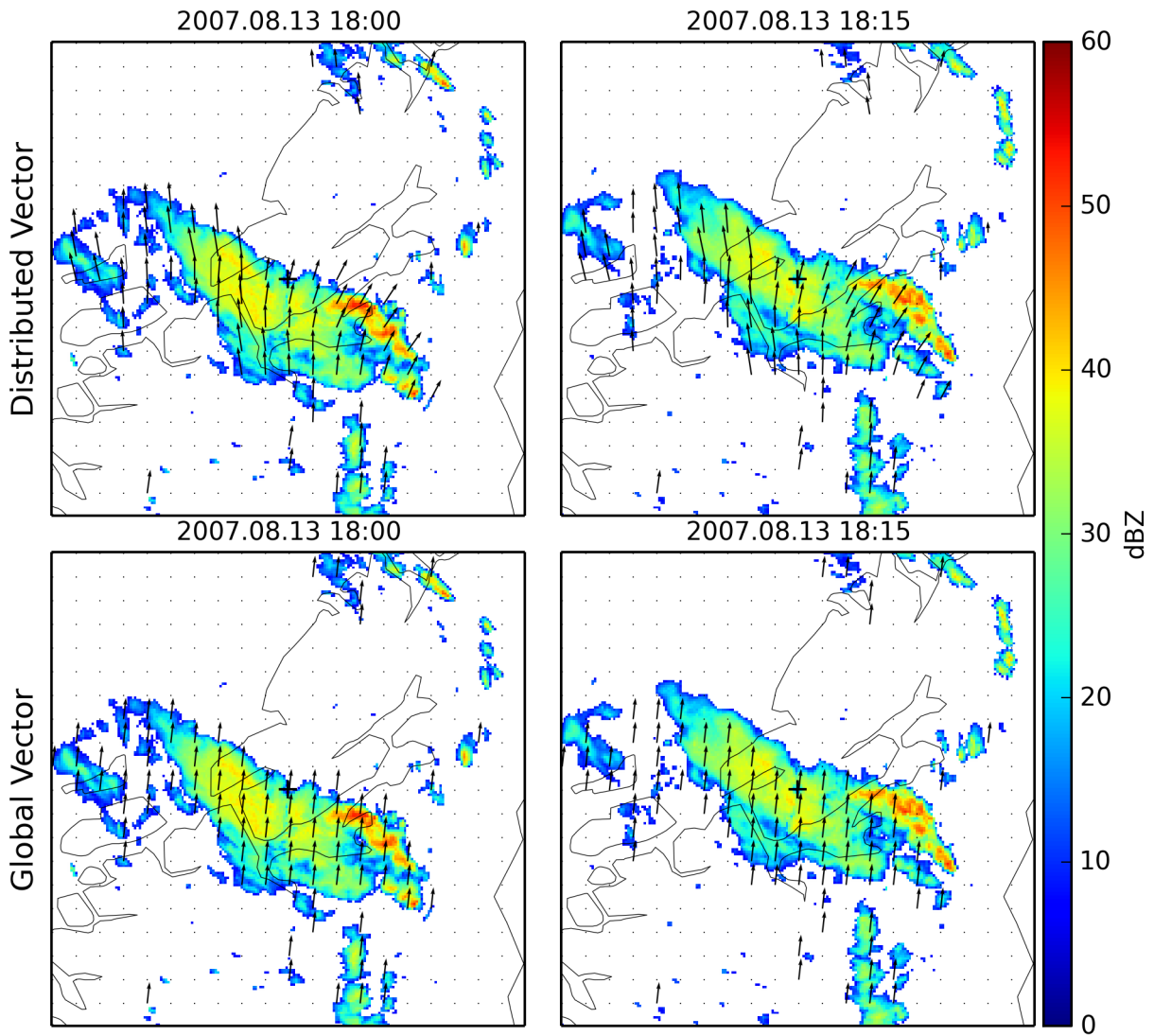
Figure 13. *Global and distributed advection vectors estimated between observed images at 18:00 and 18:15 on 13 August 2010.*
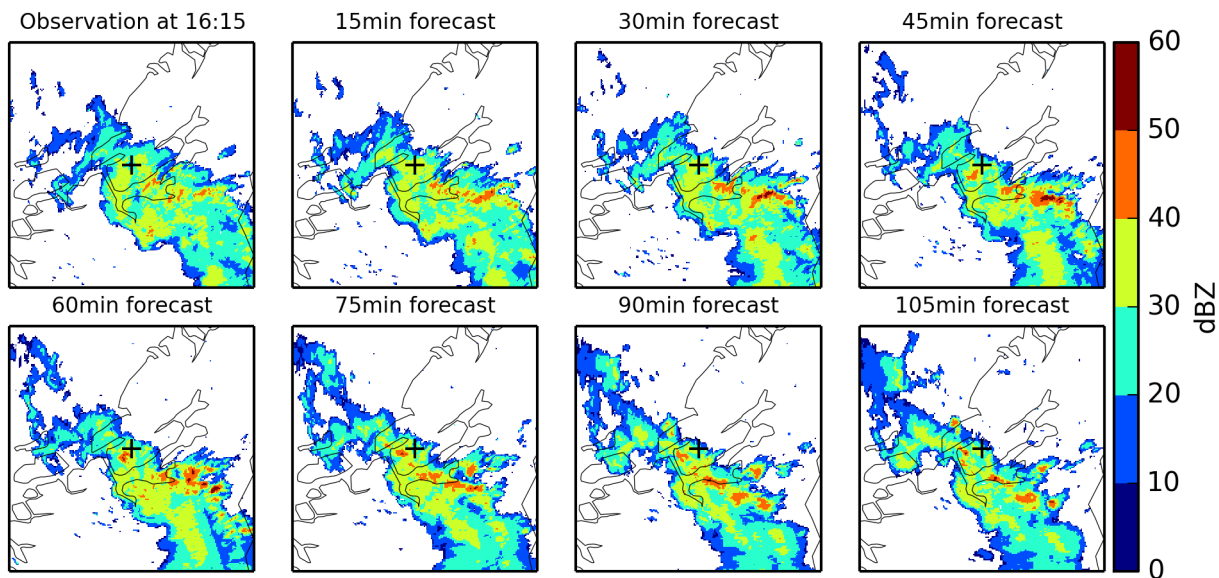
Figure 14. *Observed radar image for 28 June 2010 16:15 and forecasted images generated for the same time at different lead times. For a perfect forecast all the images should be identical.*
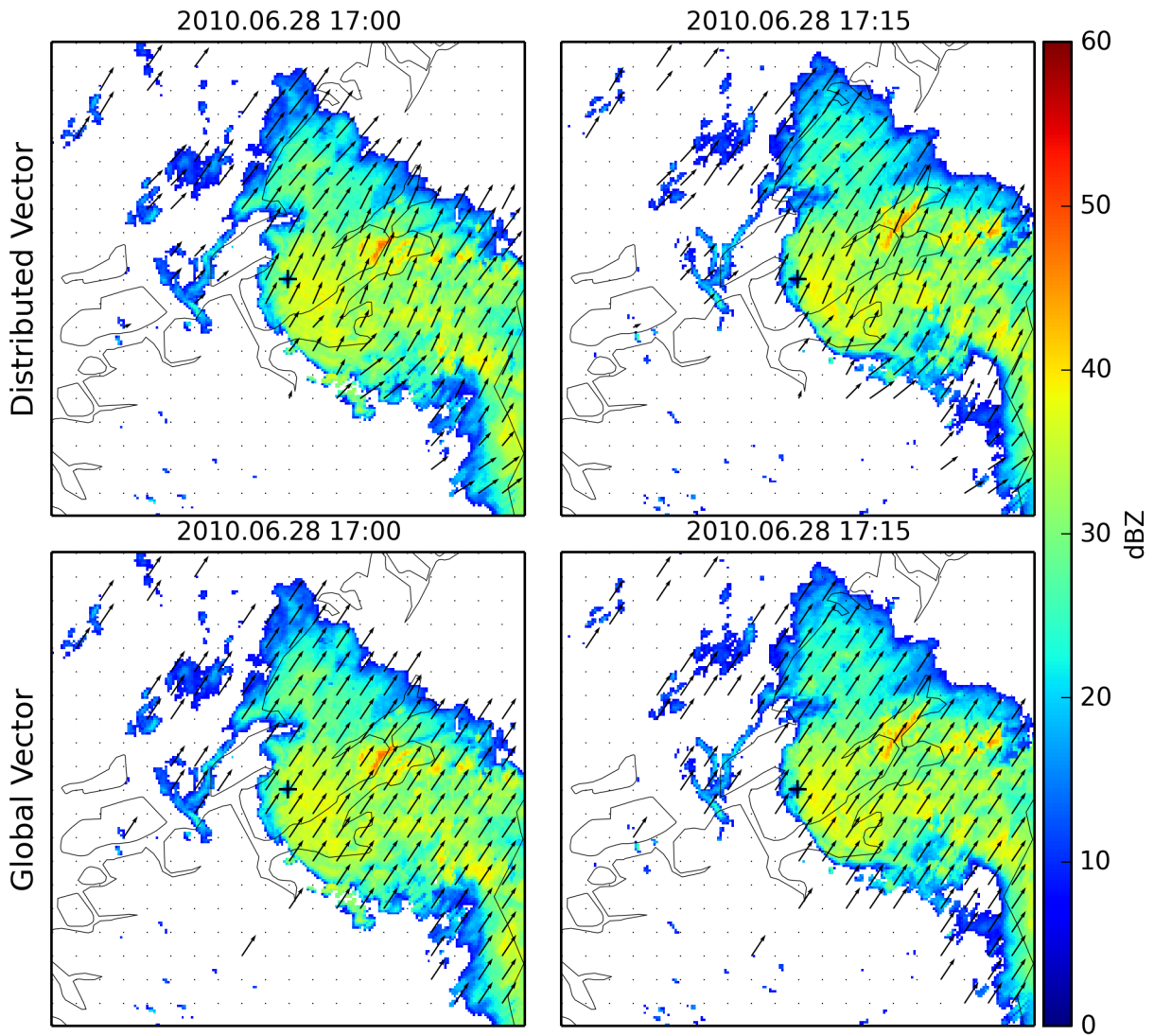
Figure 15. *Global and distributed advection vectors estimated between observed images at 17:00 and 17:15 on 28 June 2010.*

PROJECT NO.
12X846

REPORT NO.
TR A7379

VERSION
1

29 of 33

6 Summary and conclusions

In this study, a nowcasting technique based on advection of radar images has been tested on two events over central Norway. Both events, which occurred on 13 August 2007 and 28 June 2010, had convective features with high precipitation intensity. The following steps were carried out to generate forecasts for both events and evaluate the potential of the technique:

- The advection vector between successive reflectivity images was estimated. The global advection vector was estimated using a maximum cross-correlation technique while the estimation of distributed advection vectors was accomplished using an optical flow algorithm.
- Forecasts were generated for lead times of up to 2 hours with 15 min interval by advecting the radar reflectivity using the global advection vector. The extent of prediction domain is a 200x200 km^2 square region centred on the location of Rissa radar and the spatial resolution of the forecasts is 1x1 km^2.
- Six performance measures were calculated by comparing the forecasted and observed radar images. This calculation was done for several reflectivity thresholds (7, 25, 30, 35 and 40 dBZ) and verification areas (1x1, 3x3, 5x5, 7x7, 9x9 and 11x11 km^2) to analyse the scale dependence of predictability.
- For a few time steps, the global advection vectors were compared to the distributed advection vector field estimated for the same time interval in order to assess the representativeness of a spatially uniform advection.

The results from the above experiment indicate the following:

- The Lagrangian persistence model performs significantly better than the simple Eulerian persistence for both events indicating that advection is a very important factor for successfully predicting the events.
- The different performance obtained for the two events implies that storm characteristics such as rate of temporal evolution and spatial scale play a role in determining the degree of predictability.
- The performance measures calculated for the minimum reflectivity threshold of 7dBZ generally indicate good predictability of the storm envelope when compared with the same measures obtained in other studies.
- The forecast skill decreases for both events as the reflectivity threshold gets higher. This shows that more intense features in the precipitation fields are of small spatial scale and thus less predictable. This has greater implications for the application of nowcasting in urban flood warning systems since it is intense precipitation features which matter the most in such applications.
- The forecast skill improves for both events as the verification area is increased from a single pixel (1 km^2) up to an 11 x 11 pixel region (121 km^2). This incremental improvement is evident at all thresholds but gets higher for higher thresholds. Therefore, the extent of the verification area should be determined based what precision is required in terms of positioning of the intense features storm.
- The use of global advection vector could lead to erroneous forecasts at longer lead times when there are convective features with significant differential motion.
- Application of the forward advection scheme using the distributed vectors results in forecasted fields which show unrealistic dispersion in the case of divergence and intensification in the case of convergence.

7 Further research

The following issues need further research and can potentially lead to improved results through the efficient utilization of radar data in nowcasting:

- The radar data used in this study had not been corrected for errors due to non-uniform vertical profile of reflectivity, incomplete beam filling and attenuation. For generating forecasts with longer lead times, one has to advect the precipitation observed at longer distance from the radar. But it is the observations at longer distance which suffer the most from the above error sources. It is, therefore, important to check the degree to which such errors introduce 'misses' due to underestimation of reflectivity or 'false alarms' due to overestimation.

- When using images from a single-radar, the lead time of useful forecasts obtained by extrapolation of radar reflectivity is strongly limited by the maximum range of the radar. There is benefit to be gained both in terms of increased lead time and improved radar data quality when mosaics from a network of radars are used instead.

- The types of precipitation features which are of greater importance in urban flood prediction are convective features which are usually characterized by higher intensity and smaller spatial scale. According to the results obtained here and in other studies, it is such features which are more difficult to predict. It is, therefore, important to focus the evaluation of forecasting procedures against events with such features.

- Determining the typical life times of small scale convective features through studying their life cycle will help to set a limit beyond which such features should not be extrapolated. Moreover, such a study may provide knowledge on how the initiation, growth and death of these features can be used to build a model which can be included as a component in a nowcasting framework.

- The semi-Lagrangian backward advection scheme for forecasting using distributed vectors as described in German and Zawaski (2002) may be a better approach than the forward advection scheme. This scheme allows for rotation, it is almost conservative in mass and it limits the loss of power at small scales that results from interpolation.

- The distributed advection vector estimation method used in this study assigns vectors only to the pixels with precipitation. Refining the method to retrieve the vectors for all the pixels in the domain has several advantages. The main advantage is that uncertainty can be avoided by avoiding the assignment of a constant vector to each pixel for the entire period of the forecast. The refinement of the methods may be achieved by incorporating other source of meteorological information.

- In the use of either the global or distributed vectors, forecasts are generated by assuming that the advection vector field is stationary in time. It should be investigate to what extent and for which cases this assumption is valid.

8 References

Bellon, A. and I. Zawadzki (1994), Forecasting of hourly accumulations of precipitation by optimal extrapolation of radar maps, *J. Hydrol.,* 157, 211-233.

Berenguer, M., D. Sempere-Torres and G. G. S. Pegram, (2011), SBMcast – An ensemble nowcasting technique to assessthe uncertainty in rainfall forecasts by Lagrangian extrapolation, *J. Hydrol*, 404, 226-240.

Bowler, N. E. H., C. E. Pierce and A. Seed (2004), Development of a precipitation nowcasting algorithm based upon optical flow techniques, *J. Hydrol.*, 288, 74-91.

Dance, S., E. Ebert, and D. Scurrah, 2010: Thunderstorm strike probability nowcasting. *J. Atmos. Oceanic Technol.*, **27**, 79–93.

Ebert, E. E., L. J.Wilson, B. G.Brown, P. Nurmi, H. E. Brooks, J. Bally and M. Jaeneke (2004), Verification of nowcasts from WWRP Sydney 2000 Forecast Demonstration Project, *Weather and Forecasting*, 19, 73 – 96.

Fabry, F., A. Bellon, M. R. Duncan and G. L. Austin (1994), High resolution rainfall measurements by radar for very small basins: the sampling problem reexamined, *J. Hydrol.*, 161, 415-428.

*Farnebäck, G. (2003), Two-frame motion estimation based on polynomial expansion. In *Proceedings of the 13th Scandinavian conference on Image analysis* (SCIA'03), Josef Bigun and Tomas Gustavsson (Eds.). Springer-Verlag, Berlin, Heidelberg, 363-370.

Fox, N. I., and C. K. Wikle, 2005: A Bayesian quantitative precipitation nowcast scheme. *Wea. Forecasting*, 20, 264–275.

Germann, U. and I. Zawadzki (2002), Scale-Dependence of the Predictability of Precipitation from Continental Radar Images. Part I: Description of the Methodology. *Mon. Wea. Rev.*, 130, 2859–2873.

Grecu, M. and W.F. Krajewski (2000), A large-sample investigation of statistical procedures for radar-based short-term, quantitative precipitation forecasting, *J. Hydrol.*, 239(1-4), 69-84, 2000.

Han, L. Y., S. Fu, L. Zhao, Y. Zheng, H. Wang, and Y. Lin, 2009: 3D convective storm identification, tracking, and forecasting—An enhanced TITAN algorithm. *J. Atmos. Oceanic Technol.*, 26, 719–732.

Lee, H. C., A. Bellon, A. Kilambi and I. Zawadzki (2009). McGill Algorithm for Precipitation nowcasting by Lagrangian Extrapolation (MAPLE) applied to the South Korean radar network. Part 1: Sensitivity studies of the Variational Echo Tracking (VET) technique, Proceedings of the 34th Radar Conference, American Meteorological Society

Li, L., W. Schmid, and J. Joss (1995), Nowcasting of motion and growth of precipitation with radar over a complex orography, *J. Appl. Meteorol.*, 34, 1286–1300.

Marshall, J. S., and W. M. K. Palmer (1948), The distribution of raindrops with size, *J. Meteorol.*, 5, 165–166.

Pfaff, T. and A. Bárdossy (2011), Comparison of optical flow algorithms for precipitation field advection estimation, in IAHS PUBLICATION, 351, pp. 269-274, pp. 295-301, Weather Radar and Hydrology Symposium, Exeter, UK

Risholt, L. P. (2009), Kjelleroversvømmelser i Trondheim sommeren 2007, Rapport nr 571451-1, Sweco.

Ruzanski, Evan, V. Chandrasekar, Yanting Wang, 2011: The CASA Nowcasting System. *J. Atmos. Oceanic Technol.*, 28, 640–655.

Seed, A. W. (2003), A Dynamic and Spatial Scaling Approach to Advection Forecasting. *J. Appl. Meteor.*, 42, 381–388.

Thorolfsson, S. T., L. P. Risholt, O. Nilsen, A. Ellingsson, V. Kristiansen, Ø. Hagen and E. Karlsen (2008), Extreme rainfalls and damages on August 13 2007 in the city of Trondheim, Norway, in *Northern Hydrology and its global role: XXV Nordic Hydrological Conference*, pp. 295-301, Nordic Hydrological Programme, Reykjavík, Iceland.

Tsonis, A. A. and G. L. Austin (1981), An evaluation of extrapolation techniques for the short-term prediction of rain amounts. *Atmos. Ocean*, 19, 54–65.

Turner, B. J., I. Zawadzki and U. Germann (2004), Predictability of Precipitation from Continental Radar Images. Part III: Operational Nowcasting Implementation (MAPLE). *J. Appl. Meteor.*, 43, 231–248.

Wang, J. and contributing authors (2009), Overview of the Beijing 2008 Olympics project. Part I; Forecast Demonstration Project, A report to the WMO World Weather Research Programme

Wilson, J. W., N. A. Crook, C. K. Mueller, J. Sun and M. Dixon (1998), Nowcasting thunderstorms: A statusreport. *Bull. Amer. Meteor. Soc.*, 79, 2079–2099.

Wilson, J. W., Y. Feng, M. Chen and R. Roberts (2010), Nowcasting challenges during the Beijing Olympics; Successes, failures, and implications for future nowcasting systems, *Weather Forecasting*, 25, 1691-1714.

Van Horne, M. P., E. R. Vivoni, D. Entekhabi, R. N. Hoffman and C. Grassotti (2006), Evaluating the effects of image filtering in short-term radar rainfall forecasting for hydrological applications. *Meteorol. Appl.*, 13, 298-303.

Zawadzki, I., J. Morneau and R. Laprise (1994), Predictability of Precipitation Patterns: An Operational Approach. *J. Appl. Meteor.*, 33, 1562–1571.

Zahraei, A., K. Hsu, S. Sorooshian, J.J. Gourley, V. Lakshmanan, Y. Hong and T. Bellerby (2012), Quantitative Precipitation Nowcasting: A Lagrangian Pixel-Based Approach, *Atmospheric Research*, 118, 418-434.